CORRESPONDENCE

Numerical Analysis of a Pilot-Scale Fixed-Bed Reactor for Dimethyl Ether (DME) Synthesis

Daesung Song,[†] Wonjun Cho,[‡] Gibaek Lee,[§] Dal Keun Park,[†] and En Sup Yoon*[,†]

School of Chemical and Biological Engineering, Seoul National University, Seoul 151-744, Korea; LNG Technology Research Center, KOGAS, Dongchun-dong, Yeonsu-gu, Incheon 406-130, Korea; and Department of Chemical and Biological Engineering, Chungju National University, Chungju 380-702, Korea

Dimethyl ether (DME, CH_3OCH_3) is the simplest of ethers and is considered one of the leading candidates in the quest for a substitute for petroleum-based fuels. In this work, we analyzed the one-step synthesis of DME in a shell-and-tube type fixed-bed reactor. We have conducted simulations using a one-dimensional steady-state model of a heterogeneous catalyst bed. This model considered heat and mass transfer between the catalyst pellets and reactants and the effectiveness factor of the catalysts, together with the reactor cooling through the reactor tube wall. The reactor simulation was carried out under steady-state conditions. Thereafter, we compared the data of simulation results with the data obtained from the operation of a pilot-scale reactor and found acceptable agreement between the two data sets. Moreover, we analyzed effectiveness factors of the catalyst pellet and along the length of the reactor where we also analyzed temperature profiles and concentrations of the components. The analyses showed that complex reactions, when coupled with pore diffusion within the catalyst pellets, result in unusual values of the effectiveness factor along the length of the reactor. Given these results, the reactor demonstrated high performance for such variables as CO conversion and DME yield. On the contrary, operations over a high temperature range are unavoidable even though this type of reactor has been in general use. Eventually more effective cooling strategies in the operation of this type of reactor should be developed and studied.

1. Introduction

Dimethyl ether (DME), the simplest ether, is considered to be a substitute fuel that could potentially replace petroleum-based fuels.[1] The physical properties of DME are similar to liquefied petroleum gas (LPG), which could enable exploitation of existing land-based and ocean-based LPG infrastructures with minor modifications. With a cetane number of 55−60, DME is also considered a substitute for diesel fuel (cetane number 55).[2–5] Notably, when compared with diesel fuel in CIDI engine tests, the combustion of DME produced less pollutants, e.g., hydrocarbons, carbon monoxide, nitrogen oxides, and particulates.[5–9]

DME is traditionally produced by the dehydration of methanol produced from syngas, a product of natural gas reforming. This time-honored process is called the two-step method of preparing DME; however, DME can also be prepared directly from syngas (single step).[10–12] The single-step method requires only one reactor for the synthesis of DME instead of the two for the two-step process and alleviates thermodynamic limitations associated with synthesizing methanol by converting the methanol into DME and potentially enhancing overall conversion of syngas into DME. In a fixed-bed reactor, the main difficulty would be prevention of the occurrence of hot spots, since the reactions involved in the synthesis of DME are highly exothermic. Catalysts can be irreversibly deactivated when exposed to specific temperatures. Therefore, it is necessary to understand and, as a result, predict reactor behavior, including temperature profiles, under various conditions for design and scale-up of a DME synthesis process. It is not feasible to gather all the data experimentally, however, so that numerical simulations would be highly valuable in the development of such a process.

In the present study, we obtained data from a pilot plant (50 kg/day) for DME synthesis to subsequently construct and run a commercial facility (100 ton/day). We have been able to predict a DME synthesis reactor, including the additional methanol dehydration reaction (MD) (Table 1), that is operational over a higher temperature range than is a MeOH synthesis reactor (220−270 °C).[13] This prediction indicates that operations are difficult and that the control of exothermic heat within the DME synthesis reactor is a primary problem during DME synthesis. We initially developed a mathematical model to simulate a pilot-plant scale shell-and-tube type DME reactor and analyzed the one-step synthesis of DME. We then carried out the simulation of a pilot-scale fixed-bed reactor using a one-dimensional heterogeneous reactor model (under steady-state conditions) while considering heat and mass transfer between catalyst pellets and reactant gases and bearing in mind effectiveness factors of the catalysts and the cooling of the reactor through the reactor wall. A hybrid catalyst, according to our definition, consisted of catalyst pellets prepared from a mixture of fine powdered commercial methanol synthesis catalyst ($CuO/ZnO/Al_2O_3$) and

Table 1. Kinetic Parameters and Equilibrium Constants[a]

	$A(i)$	$B(i)$
k_1	1.65	36696
K_2	3610	0
K_3	0.37	17197
K_4	7.14×10^{-11}	124119
k_5	1.09×10^{10}	−94765
K_{CH_3OH}	0.00079	70500
k_6	3.7×10^{10}	−105000
K_{H_2O}	0.084	41100

[a] Parameter $= A(i) \exp(B(i)/RT)$.

* To whom correspondence should be addressed. Tel.: +82-2-880-1581. Fax: +82-2-872-1581. E-mail: esyoon@snu.ac.kr.
[†] Seoul National University.
[‡] LNG Technology Research Center.
[§] Chungju National University.

10.1021/ie071589e CCC: $40.75
Published on Web 05/24/2008

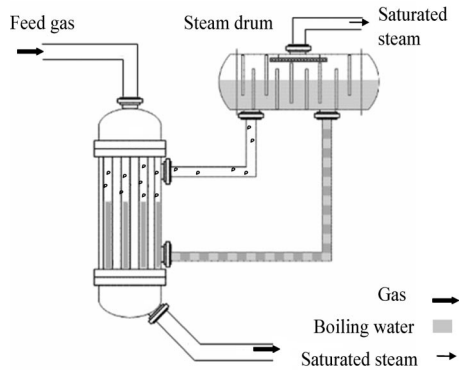

Figure 1. Reactor flow sheet for synthesis of DME.

a fine powdered methanol dehydration catalyst (γ-alumina) used in the pilot plant. Thus, the active sites for the synthesis of methanol and for its dehydration are intermixed within the catalyst pellets. By using the simulator developed in this study, we compared the results from the operation of a pilot-scale DME reactor with the simulation ones, e.g., temperature profile, CO conversion, DME yield, and out-stream composition, and we analyzed effectiveness factors of the catalyst pellet and along the length of the reactor. Additionally along the length of the reactor, we analyzed both the temperature profile and the concentration-of-components profile.

2. Development of the Reactor Model

2.1. Reactor Summary. The reactor flow sheet for DME synthesis is shown in Figure 1. The catalyst is packed in vertical tubes, and boiling water surrounds a stationary tube bundle. Reaction heat is transferred to the boiling water, and steam is produced. Vaporous bubbles of gas are generated at the heating surface, rise through the mass of liquid, and disengage from the surface of the liquid. Vapor accumulates in a vapor space over the liquid; a vapor outlet from the vapor space removes the vapor as rapidly as it is formed. This type of boiling is termed pool boiling of a saturated liquid. Typical operating conditions are approximately 280 °C and 50 bar. The reactor temperature is controlled by controlling the pressure of the boiling water.

2.2. Reactor Model Assumptions. For modeling the reactor, the following assumptions are made: (i) a one-dimensional heterogeneous model, (ii) negligible radial temperature gradient and axial dispersion in the reactor tube, (iii) insignificant radial temperature gradient in catalyst pellets because the conductivity of the catalyst pellets are sufficiently high as to discount any temperature difference between core and surface, and (iv) dynamics of catalyst deactivation that are ignored because of a large time constant.

2.3. Reaction Kinetics. The preparation of DME from syngas is represented by three catalytic reactions as shown:[14]

$$CO_2 + 3H_2 \leftrightarrow CH_3OH + H_2O \quad (1a)$$

$$CO + H_2O \leftrightarrow CO_2 + H_2 \quad (1b)$$

$$2CH_3OH \leftrightarrow CH_3OCH_3 + H_2O \quad (1c)$$

Reaction 1a corresponds to synthesis of methanol from carbon dioxide and hydrogen, the methanol synthesis reaction (MS). Reaction 1b is the reverse water gas shift reaction (RWGS). Each of these reactions is catalyzed by the methanol synthesis catalyst ($CuO/ZnO/Al_2O_3$). Reaction 1c, the methanol dehydration reaction (MD), is catalyzed by an acidic catalyst (γ-alumina). A combination of these three reactions explains the other schemes of preparation of DME from syngas. We also use the reaction rate equations as follows.[15,16]

$$r_{MS} = \frac{k_1(p_{H_2}p_{CO_2})[1 - (1/K_{eqm1})(p_{CH_3OH}p_{H_2O})/(p_{CO_2}p_{H_2}^3)]}{(1 + K_2(p_{H_2O}/p_{H_2}) + \sqrt{K_3 p_{H_2}} + K_4 p_{H_2O})^3} \quad (2a)$$

$$r_{RWGS} = \frac{k_5 p_{CO_2}[1 - K_{eqm2}(p_{CO}p_{H_2O}/p_{CO_2}p_{H_2})]}{1 + K_2(p_{H_2O}/p_{H_2}) + \sqrt{K_3 p_{H_2}} + K_4 p_{H_2O}} \quad (2b)$$

$$r_{MD} = k_6 K_{CH_3OH}{}^2 \left[\frac{C_{CH_3OH}{}^2 - (C_{H_2O}C_{DME}/K_{eqm3})}{(1 + 2\sqrt{K_{CH_3OH}C_{CH_3OH}} + K_{H_2O}C_{H_2O})^4} \right] \quad (2c)$$

The values of the kinetic parameters in the kinetic expressions are summarized in Table 1. The equilibrium constant of each reaction is taken from the literature as follows.[17,18]

$$\log_{10} K_{eqm1} = \frac{3066}{T} - 10.592 \quad (3a)$$

$$\log_{10} \frac{1}{K_{eqm2}} = -\frac{2073}{T} + 2.029 \quad (3b)$$

$$\log_{10} K_{eqm3} = \frac{10194}{T} - 13.91 \quad (3c)$$

2.4. Heat and Mass Transfer on the Catalyst Surface. Because of the highly exothermic nature of the reactions, the temperature of catalyst pellets can differ from that of the bulk stream of the reactants. Therefore, we investigated heat transfer on the surface of catalyst pellets and employed conventional expressions (eq 4) for the heat transfer coefficient.[19–21]

$$N_{Nu} = \frac{h_p d_p}{k_g} = 2 + 0.6 N_{Re,sph}{}^{0.5} N_{Pr}{}^{1/3}$$

$$N_{Re,sph} = \frac{d_p v \rho}{\mu}$$

$$N_{Pr} = \frac{C_{p,g}\mu}{k_g} \quad (4)$$

The temperature of the catalyst particles should satisfy the energy balance between heat transfer and heat of reaction; at a steady state, the reaction heat should equal the heat transferred between the surface of the catalyst and the reaction fluid.

$$\sum_i r_i \Delta H_r g_{cat} = h_p A_p (T_p - T_f) \quad (5)$$

Since both diffusion and reaction steps are involved in the reactor, the relative rates of each step are important. When the reaction rate is relatively rapid compared to the rate of diffusion, the process is said to be diffusion-controlled. In contrast, the process is said to be reaction-controlled when the rate of mass transfer is limited by the reaction step. Therefore, we investigated mass transfer on the catalyst and employed conventional

Table 2. Methods Used for Calculating Physicochemical Properties

property	method
gas viscosity	Lucas[25]
gas conductivity	Steil−Thodos[26]
binary diffusion coefficient, components *i* and *j*	Fuller−Schettler−Gidding (FSG)[26]
mixed-gas heat capacity	ideal gas[25]
gas compressibility factor for reactor inside	Peng−Robinson[25]

Table 3. Properties of the Catalyst and Pilot-Plant Scale Reactor

catalyst	density (kg/m3)	1783.5
	porosity (%)	45.53
	pore tortuosity	1.69
	mass (kg)	7.85
	pellet diameter (m)	0.006
reactor	tube diameter (m)	0.03
	length (m)	1.6
	tube number	7

expressions (eq 6) for the diffusion rate of the diffusing components and the mass transfer coefficient.[20]

$$W_{\mathrm{Ar}.i} = k_{ci}(C_{\mathrm{A0}.i} - C_{\mathrm{As}.i})$$
$$N_{\mathrm{Sh}} = \frac{k_{ci}d_{\mathrm{p}}}{D_{i,j}} = 1.17N_{\mathrm{Re}}^{0.585}N_{\mathrm{Sc}}^{1/3}$$
$$N_{\mathrm{Re}} = \frac{d_{\mathrm{p}}v\rho}{\mu}$$
$$N_{\mathrm{Sc}} = \frac{\mu}{\rho D_{i,j}} \tag{6}$$

Then, we decided whether the process is diffusion-controlled or reaction-controlled.

2.5. Effectiveness Factor. The observed rate of reaction can differ from the rate of reaction at surface concentration because of pore diffusion in the catalyst pellets where their diameter is of the order of several millimeters. The effectiveness factor can be calculated from eq 7, i.e., the ratio of the observed rate of reaction to the rate of reaction at surface concentration. If $\eta \rightarrow 1$, mass transfer is fast compared with kinetics. If η is small, reaction kinetics is fast compared with diffusion mass transfer.

$$\eta_{\mathrm{MS\backslash WGS\backslash MD}} = \frac{4\pi R_{\mathrm{p}}{}^2 D_{\mathrm{eff},j}\left(-\frac{\mathrm{d}c}{\mathrm{d}r}\right)_{r=R}}{\frac{4}{3}\pi R_{\mathrm{p}}{}^3 r_{\mathrm{MS\backslash WGS\backslash MD}}} \tag{7}$$

We chose not to consider energy balance within and assumed that a radial temperature gradient within a catalyst pellet top would be negligible. In a spherical catalyst pellet, the concentration of the reactants and products can be obtained by solving the partial differential equations as follows.[22,23]

$$\frac{\mathrm{d}^2C_{\mathrm{H_2}}}{\mathrm{d}r^2} + \frac{2}{r}\frac{\mathrm{d}C_{\mathrm{H_2}}}{\mathrm{d}r} = \frac{3\rho_{\mathrm{p_1}}}{D_{\mathrm{eff.H_2}}}r_{\mathrm{CO_2}} + \frac{\rho_{\mathrm{p_1}}}{D_{\mathrm{eff.H_2}}}r_{\mathrm{RWGS}} \tag{8a}$$

$$\frac{\mathrm{d}^2C_{\mathrm{CO}}}{\mathrm{d}r^2} + \frac{2}{r}\frac{\mathrm{d}C_{\mathrm{CO}}}{\mathrm{d}r} = -\frac{\rho_{\mathrm{p_1}}}{D_{\mathrm{eff.CO}}}r_{\mathrm{RWGS}} \tag{8b}$$

$$\frac{\mathrm{d}^2C_{\mathrm{CO_2}}}{\mathrm{d}r^2} + \frac{2}{r}\frac{\mathrm{d}C_{\mathrm{CO_2}}}{\mathrm{d}r} = \frac{\rho_{\mathrm{p_1}}}{D_{\mathrm{eff.CO_2}}}r_{\mathrm{CO_2}} + \frac{\rho_{\mathrm{p_1}}}{D_{\mathrm{eff.CO_2}}}r_{\mathrm{RWGS}} \tag{8c}$$

$$\frac{\mathrm{d}^2C_{\mathrm{H_2O}}}{\mathrm{d}r^2} + \frac{2}{r}\frac{\mathrm{d}C_{\mathrm{H_2O}}}{\mathrm{d}r} = -\frac{\rho_{\mathrm{p_1}}}{D_{\mathrm{eff.H_2O}}}r_{\mathrm{CO_2}} - \frac{\rho_{\mathrm{p_1}}}{D_{\mathrm{eff.H_2O}}}r_{\mathrm{RWGS}} - \frac{\rho_{\mathrm{p_2}}}{2D_{\mathrm{eff.H_2O}}}r_{\mathrm{MeOH}} \tag{8d}$$

$$\frac{\mathrm{d}^2C_{\mathrm{DME}}}{\mathrm{d}r^2} + \frac{2}{r}\frac{\mathrm{d}C_{\mathrm{DME}}}{\mathrm{d}r} = -\frac{\rho_{\mathrm{p_2}}}{2D_{\mathrm{eff.DME}}}r_{\mathrm{MeOH}} \tag{8e}$$

$$\frac{\mathrm{d}^2C_{\mathrm{MeOH}}}{\mathrm{d}r^2} + \frac{2}{r}\frac{\mathrm{d}C_{\mathrm{MeOH}}}{\mathrm{d}r} = -\frac{\rho_{\mathrm{p_1}}}{D_{\mathrm{eff.MeOH}}}r_{\mathrm{CO_2}} + \frac{\rho_{\mathrm{p_2}}}{D_{\mathrm{eff.MeOH}}}r_{\mathrm{MeOH}} \tag{8f}$$

at boundary conditions $r = R$, $C = C_{\mathrm{As}.i}$ and $r = 0$, $\mathrm{d}C/\mathrm{d}r = 0$. The effective diffusivity of the gases through the porous catalyst pellets was estimated from the molecular diffusivity, porosity, and tortuosity of the pores using eq 9.

$$D_{\mathrm{eff}.i} = D_i\frac{\varepsilon}{\tau} \tag{9}$$

where Di= molecular diffusivity, ε = void fraction (porosity), and τ = tortuosity. The solutions to these equations provide the concentration profiles of the gas species in the catalyst pellets together with the global reaction rates.

2.6. Heat Transfer between Tubes and Shell. The heat generated from the chemical reactions in the catalyst is transferred to the gases flowing through the reactor tubes and then to the cooling medium on the shell side of the reactor. Equation 10 holds for the whole reactor, as well as for any given reactor section. The temperature rise of the reactants is calculated by subtracting the heat transferred to the coolant from the heat generated by the chemical reactions.

$$\left(\sum_i r_i\Delta H_{\mathrm{r}}g_{\mathrm{cat}} - U_{\mathrm{o}}A_{\mathrm{t}}(T_{\mathrm{f}} - T_{\mathrm{o}})\right) = C_{p,\mathrm{fluid}}m_{\mathrm{f}}\Delta T_{\mathrm{f}} \tag{10}$$

To estimate the heat transfer coefficient (eq 11) or U, it is necessary to know both the shell-side and tube-side heat transfer coefficients.

$$U_{\mathrm{o}} = \frac{1}{\frac{1}{h_{\mathrm{i}}}\left(\frac{D_{\mathrm{o}}}{D_{\mathrm{ti}}}\right) + \frac{x_{\mathrm{w}}}{k_{\mathrm{m}}}\left(\frac{D_{\mathrm{o}}}{D_{\mathrm{L}}}\right) + \frac{1}{h_{\mathrm{o}}} + \frac{D_{\mathrm{o}}}{D_{\mathrm{ti}}}\frac{1}{h_{\mathrm{di}}} + \frac{1}{h_{\mathrm{do}}}} \tag{11}$$

In the case of pool boiling of a saturated liquid, we adopted a value for the heat transfer coefficient, h_{o}= 5678 W/(m^2 °C);[24] however, the presence of catalyst pellets complicates the estimation of the heat transfer coefficient on the tube side. Because we do not have experimental values for the tube-side heat transfer coefficient, we selected a correlation (eq 12) to estimate the tube-side heat transfer coefficient.[19]

$$h_{\mathrm{i}} = \left(\frac{1}{\frac{1}{h_{\mathrm{r}} + 2k_{\mathrm{ew}}^0/d_{\mathrm{p}} + a_{\mathrm{w}}C_{p,\mathrm{g}}\rho_{\mathrm{g}}\nu} + \frac{1}{h_{\mathrm{packet}}}}\right) \tag{12}$$
$$h_{\mathrm{packet}} = 1.13\left(\frac{k_{\mathrm{e}}^0\rho_{\mathrm{p}}(1-\varepsilon_{\mathrm{mf}})C_{p,\mathrm{s}}}{\tau_{\mathrm{t}}}\right)^{0.5}$$
$$k_{\mathrm{ew}}^0 = \varepsilon_{\mathrm{w}}k_{\mathrm{g}} + (1-\varepsilon_{\mathrm{w}})k_{\mathrm{s}}\left(\frac{1}{\phi_{\mathrm{w}}(k_{\mathrm{s}}/k_{\mathrm{g}}) + 1/3}\right)$$
$$k_{\mathrm{e}}^0 = \varepsilon_{\mathrm{mf}}k_{\mathrm{g}} + (1-\varepsilon_{\mathrm{mf}})k_{\mathrm{s}}\left(\frac{1}{\phi_{\mathrm{b}}(k_{\mathrm{s}}/k_{\mathrm{g}}) + 2/3}\right)$$
$$a_{\mathrm{w}} = 0.05,\ h_{\mathrm{r}}(\mathrm{radiation}) = 0$$

2.7. Pressure Drop in the Tube. Gases flowing through beds of solid particles encounter resistance as the result of the total drag of all particles within the bed. A measure of the pressure drop, therefore, is taken by the following Ergun equation.[24]

$$\frac{\Delta p}{L} = \frac{150\mu_{\mathrm{a}}(1-\varepsilon)^2u_{\mathrm{o}}}{\varepsilon^3d_{\mathrm{p}}{}^2} + \frac{1.75(1-\varepsilon)\rho u_{\mathrm{o}}{}^2}{\varepsilon^3d_{\mathrm{p}}} \tag{13}$$

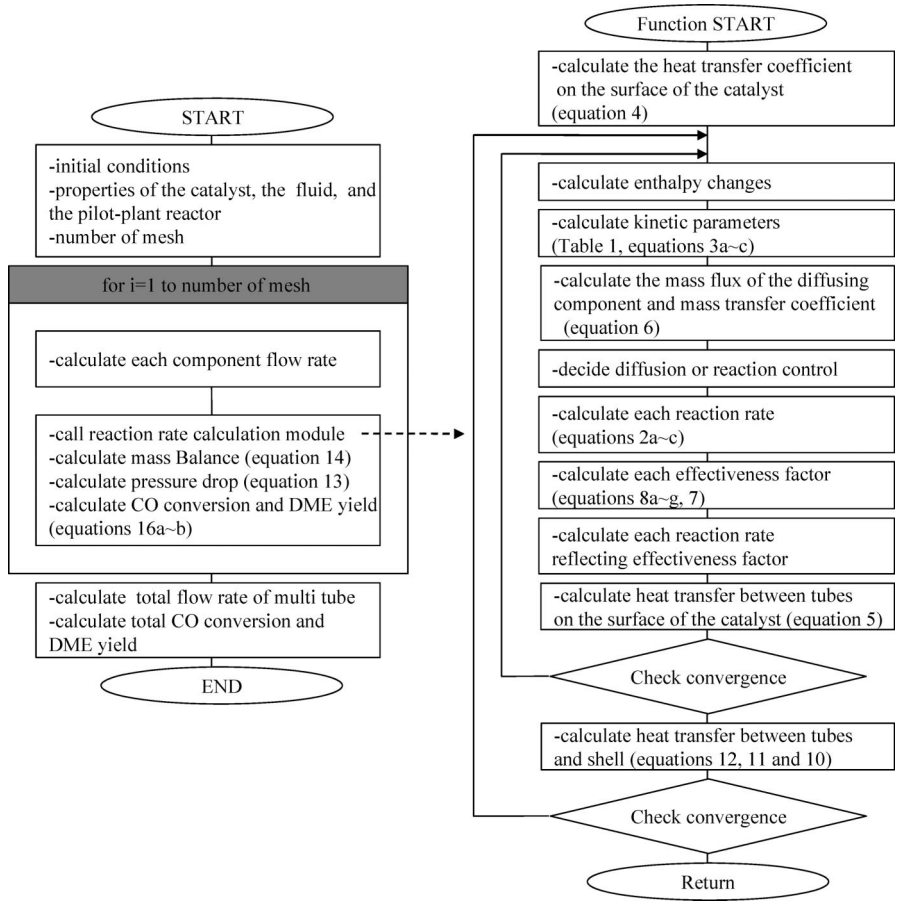

Figure 2. Flow sheet of main module and reaction rate calculation module.

2.8. Simulation of the Reactor. Equation 14 is used to calculate the mass flow rate profile in the tube of the reactor.[23]

$$\frac{dF_i}{dz} = \rho_b \frac{\pi D_{ti}^2}{4} \sum_{j=1}^{n_r} \gamma_{ij} r_j \quad i = 1, 2, ..., n_c \tag{14}$$

To solve the ordinary differential equation (ODE) above, the axial length of the reactor tube was divided into 1000 sections. In many simulations, a mesh number of less than 1000 sections could not converge easily. On the contrary, a mesh number greater than 1000 sections would converge but required more time.

The methods used for calculating the physicochemical properties needed for our simulation are provided in Table 2. Binary diffusion coefficients for a multicomponent system were calculated on the assumption that each component in the bulk fluid penetrates into syngas film consisting of main components H_2 and CO in the reactor on the surface of a catalyst. The binary diffusion coefficients between each component in bulk fluid and syngas film were estimated by the Fuller, Schettler, and Giddings' (FSG) eq 15.[26]

$$D_{i,j} = \frac{10^{-4} T^{1.75} (M_i^{-1})^{1/2}}{P_{atm} (\sum v_i^{1/3} + \sum v_j^{1/3})^2} \tag{15}$$

where j = syngas film (H_2 and CO).

The diffusion volume of syngas film, v_j, was calculated with respect to the mole ratio of H_2 and CO in the reactor. The diffusion volume of methanol and dimethyl ether had to be calculated by the summation of the atomic diffusion volume increments. Values of $\sum v_{MeOH} = 29.9$ cm^3 mol^{-1} and $\sum v_{DME} = 50.36$ cm^3 mol^{-1} were used in the calculations.[25] The diffusion volumes of the other components are reported by Fuller et al.[27] To estimate the gas compressibility factor, Van der Waals one-fluid mixing rule and vapor−liquid equilibrium (VLE data of DETHERM databank were used.

We first set initial conditions, properties of the catalyst, the fluid, and the pilot-plant reactor, and the number of meshes and then calculated the reaction rates with the use of the correlations listed in Section 2.3. For this calculation, the heat and mass transfer on the surface of the catalyst described in Section 2.4 and the effectiveness factor described in Section 2.5 were incorporated and reflected their effects on reaction rates. The correlations of Section 2.6 were then used for calculating the reactor temperature in each section. Iterative procedures for determining the temperature and reaction rates in each section were necessary, because the temperature and reaction rates are interdependent. After determining the temperature in a given section of the tube, the mass balance in each such section could be calculated using eq 14 and the simulation could be allowed to proceed to the next step. The procedure flowchart is depicted in Figure 2, and this is discussed in Section 2, development of the reactor model.

We used the following correlations to evaluate the reactor performance of the CO conversion and the DME yield:

$$CO_{conversion} = \frac{CO_{in} - CO_{out}}{CO_{in}} \times 100 \tag{16a}$$

$$DME_{yield} = \frac{DME_{out} \times 2}{CO_{in} - CO_{out}} \times 100 \tag{16b}$$

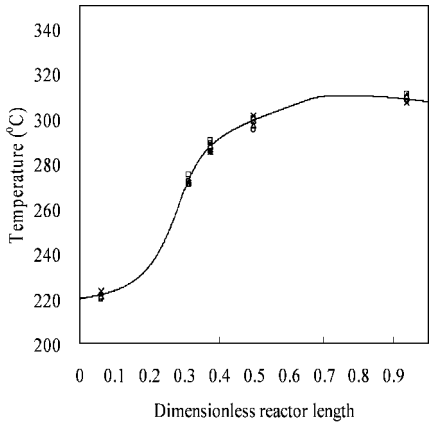

Figure 3. Simulated temperature profile and experimental data along the reactor length.

3. Results and Discussion

Using the simulator that we developed, the behavior of a pilot-scale DME reactor could be studied. The base condition of a pilot-scale DME reactor was as follows: feed composition: $yH_2 = 0.589$, $yCO = 0.391$, $yCO_2 = 0.002$, $yCH_4 = 0.0025$ and $yH_2O = 0.0157$, $yCH_3OH = 0$, $yCH_3OCH_3 = 0$; GHSV = 2000 h^{-1}; feed temperature = 220 °C; reactor pressure = 50 bar; H_2/CO ratio = 1.5:1; and temperature of boiling water = 215 °C.

The hybrid catalyst consists of the methanol synthesis and methanol dehydration components, at a ratio of 8:2 synthesis/dehydration. The properties of the catalyst and the information concerning the pilot-plant scale reactor are shown in Table 3. This information was used for the reactor simulation. We compared the experimental data obtained from the pilot-scale fixed-bed reactor with the simulation results. Moreover, we analyzed effectiveness factors of the catalyst pellet and along the length of the reactor. Additionally along the length of reactor, we analyzed both the temperature profile and the concentration-of-components profile.

3.1. Comparison of Experimental and Simulation Results. Figure 3 shows the simulated temperature profile and reactor temperatures measured for five operations as shown in Table 3 at five points (0.1, 0.5, 0.6, 0.8, and 1.6 m). Although the simulated temperature profile has an error range of ±8.8 °C, this simulator can predict the temperature profile of the reactor extremely accurately, thus helping to control the reactor temperature and preventing irreversible deactivation of the catalysts. Table 4 shows the simulation result with corresponding pilot plant reactor data when measured at a steady state and indicates that CO conversion and DME yields decrease after each operation. Catalyst deactivation during operations may contribute to this observation. Nonetheless, there is good agreement between the simulations result and the pilot plant reactor data.

3.2. Effectiveness Factors Analysis of the Catalyst Pellet and Along the Length of the Reactor. The simulator evaluates effectiveness factors of the catalyst pellet by solving the mass balance equations for pore diffusion and chemical reactions within the pellets. We used the reaction conditions at the entrance zone of the reactor and observed a strong influence of pore diffusion on the reaction rate. Figure 4 shows that all three reactions occur within the same catalyst pellet. Although the reaction rate of the water gas shift reaction (WGS) decreases toward the center of the catalyst pellet as a result of pore diffusion effects, the reaction rates of methanol synthesis (MS) and methanol dehydration (MD) in the core region of catalyst pellets are higher than those near the pellet surface. Since reactions 1a, 1b, and 1c involved in methanol synthesis and DME are interrelated in a complex way, including through pore diffusion, their rates within the catalyst pellet reflect an interaction of the mass transfer and chemical reactions, as well as variations in species concentrations within the catalyst. Once the reaction profiles in the catalyst pellet were studied, we evaluated effectiveness factors for the three reactions along the axis of the reactor toward the reactor outlet. Figure 5 shows the lines of the effectiveness factor of the methanol synthesis reaction (MS), the water gas shift reaction (WGS), and the methanol dehydration reaction (MD). All of the reactions were active and demonstrated little effect of pore diffusion in the hybrid catalyst. Therefore, the effectiveness factor for the methanol dehydration reaction (MD) exceeded 100% in the entrance zone of the reactor, since DME is produced in a vigorous manner within the inner catalyst, and for methanol, the synthesis is also above 100% in the entrance zone of the reactor. Beyond the entrance zone of the reactor, the effectiveness factor for methanol synthesis increases to around 100%, while that of the water gas shift reaction increases to around 250%. Moreover, the effectiveness factor for the DME synthesis reaction is always above 50% beyond the entrance zone of the reactor.

3.3. Concentration-of-Components and Temperature Profile Analysis. The concentration-of-components and temperature profiles are shown in Figure 6. The maximum temperature in the reactor is 310 °C. The active sites for methanol synthesis and methanol dehydration coexist and achieve synergic effects because of their proximity. As shown in Figure 6, maintaining a uniform temperature along the reactor length is a major problem because of the highly exothermic nature of the reactions involved in DME synthesis, even with the advanced shell-and-tube type reactor design.

4. Conclusion

In this work, we have detailed our development of a simulator shell-and-tube type pilot-scale fixed-bed reactor for the single-step synthesis of DME from syngas and applied a one-dimensional heterogeneous model for a steady-state condition. We applied this model to a pilot-scale reactor and found good agreement between simulation and experimental results. We were also able to predict the operational behavior of the reactor by using the simulator. Thus, we were able to predict the temperature profile of the reactor and prevent irreversible deactivation of catalysts, further allowing stable and optimized operation conditions and scale-up of a DME synthesis reactor. Moreover, we examined the behavior of the reactor using a hybrid catalyst. We determined that complex reactions are coupled with pore diffusion within the catalyst pellets, resulting in unusual effectiveness factor values. Therefore, the reactor provided such higher performances as CO conversion and DME yields. On the contrary, operation at high temperature (maximum temperature, 310 °C) is inevitable even though this reactor type has been commercially well-developed. In the future, a more effectively controlled cooling strategy must be developed and studied. Additionally, we used the values of physicochemical properties at typical operating conditions (280 °C, 50 bar) for this simulation. The physicochemical properties such as viscosity, density, and conductivity are usually dependent on temperature. Therefore, errors may occur. Errors that occurred especially in the range of 220−240 °C can slightly affect the reactor performance. In the next study, we will calculate the

Table 4. Comparison of the Simulation Results and Pilot-Plant Reactor Data

property	simulation result	pilot-plant result 1	pilot-plant result 2	pilot-plant result 3	pilot-plant result 4	pilot-plant result 5
CO conversion	39.85	39.4	38.93	37.92	37.39	36.27
DME yield	50.58	50.02	49.41	48.01	47.20	45.39
mole %						
yH_2	54.96	54.74	56	54	57	53
yCO	29.6	29.8	29.9	30.3	28.4	32.61
yCO_2	6.79	6.68	5.42	7.31	6.17	5.88
yCH_4	0.31	0.31	0.30	0.24	0.31	0.31
yH_2O	0.43	0.41	0.39	0.36	0.34	0.31
yCH_3OCH_3	4.97	4.78	4.71	4.44	4.29	3.98
yCH_3OH	2.94	3.02	3.12	3.33	3.45	3.71
byproduct		0.26	0.16	0.02	0.04	0.2

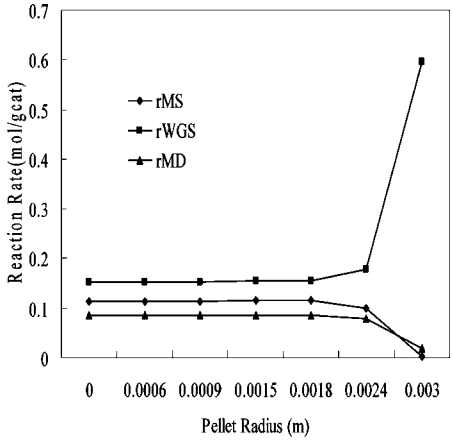

Figure 4. Reaction rates for CO_2 hydrogenation, water gas shift, and methanol dehydration in a hybrid catalyst.

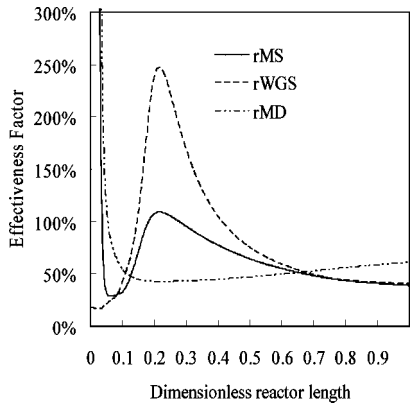

Figure 5. Effectiveness factor versus axial distance along the reactor length.

physicochemical properties as functions of temperature to increase the simulation accuracy.

Acknowledgment

The support provided for this study came from KOGAS (Korea Gas Corporation). BK21 (Brain Korea21) support is gratefully acknowledged.

Nomenclature

A_p = surface area of the catalyst, m^2
A_t = external surface area of the tubes, m^2
$C_{A0.i}$ = concentration of component i in reactants fluid, kmol m^{-3}
$C_{As.i}$ = concentration of component i on the catalyst surface, kmol m^{-3}
$C_{p,g}$, $C_{p,fluid}$ = specific heat of fluid, cal mol^{-1} K^{-1}
$C_{p,s}$, $C_{p,w}$ = specific heat of particles at the surface and of cooling water, respectively, cal mol^{-1} K^{-1}

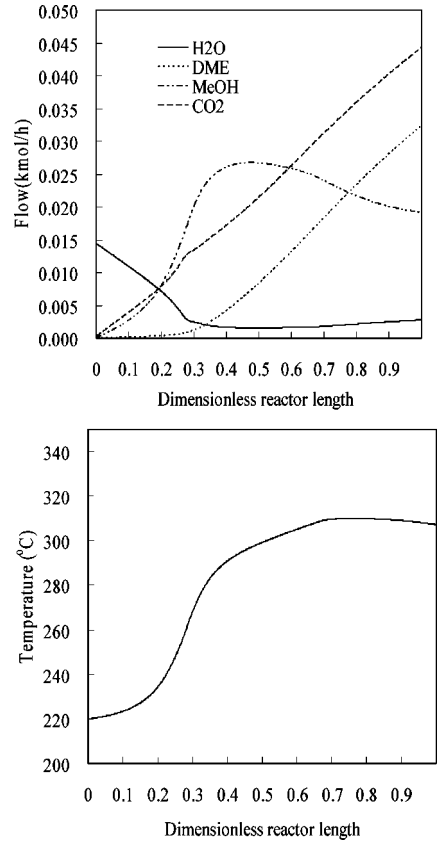

Figure 6. Simulated concentration of components and temperature profile along the reactor length.

dH_r, ΔH_r = heat of reaction, kJ mol^{-1}
d_p = particle diameter, m
$D_{i,j}$ = binary diffusivity of gas, cm^2 s^{-1}
$D_{eff.i}$ = effective diffusivity of component i within a catalyst pellet, m^2 h^{-1}
D_{ti},D_o = tube inside and outside diameter, m
D_L = equivalent diameter of a tube, m
F_i = molar flow rate of species i, kmol h^{-1}
g_{cat1}, g_{cat2} = mass of the MeOH synthesis catalyst and the MeOH dehydration catalyst, g
h_{di},h_{do} = fouling resistance of a tube side and a shell side at heat transfer, kJ h^{-1} m^{-2} K^{-1}
h_i, h_o = film coefficient of a tube inside and outside, J m^{-2} h^{-1} °C $^{-1}$
h_p = film coefficient at heat transfer on a catalyst pellet, J m^{-2} h^{-1} °C $^{-1}$
h_{packet} = film coefficient in a packet, J m^{-2} h^{-1} °C $^{-1}$
h_r = heat transfer coefficient for a radiation, J m^{-2} h^{-1} °C $^{-1}$
k_{ci} = mass transfer coefficient of component i, m s^{-1}
k_e^0, k_{ew}^0 = effective thermal conductivity at the fixed bed and the wall region, J m^{-2} h^{-1} °C $^{-1}$

k_g = fluid thermal conductivity, J m^{-2} h^{-1} °C $^{-1}$
k_i = reaction rate constants
k_m, k_s = heat conductivity of a wall and a particle, J m^{-2} h^{-1} °C $^{-1}$
K_i, $K_{eqm,j}$ = adsorption constant and equilibrium constant of reaction j, respectively
L = height of the bed, m
m_f = mole flow rate of the fluid in the tube, gmol h^{-1}
M_i = molecular weight of component i, g mol^{-1}
n_c, n_r = number of components and reactions
N_{Nu} = Nusselt number
N_{Pr} = Prandtl number
N_{Re} = Reynolds number
$N_{Re,sph}$ = particle Reynolds number
N_{Sc} = Schmidt number
N_{Sh} = Sherwood number
Δp = pressure drop, bar
P_{atm} = pressure in atmospheres, 1.013 bar
P_i = partial pressure of component i
r = radial distance in the catalyst, m
r_i = reaction rate of i reactions, mol $gcat^{-1}$ h^{-1}
r_{MS} = reaction rate of the methanol synthesis reaction, mol $gcat^{-1}$ h^{-1}
r_{RWGS} = reaction rate of the reverse water gas shift reaction, mol $gcat^{-1}$ h^{-1}
r_{WGS} = reaction rate of the water gas shift reaction, mol $gcat^{-1}$ h^{-1}
r_{MD} = reaction rate of the methanol dehydration reaction, mol $gcat^{-1}$ h^{-1}
r_j = reaction rate of the jth reaction, mol $gcat^{-1}$ h^{-1}
R = gas constant, 8.314 J mol^{-1} K^{-1}
R_P = particle radius, m
T_f = fluid temperature, K
T_o, T_p = temperature of cooling water and catalyst, K
ΔT_f = temperature difference of fluid, K
$W_{Ar,i}$ = diffusion rate of component i, kmol m^{-2} s^{-1}
u_o = volumetric average fluid velocity, m s^{-1}
U_o = overall heat transfer coefficient, J m^{-2} h^{-1} °C $^{-1}$
x_w = thickness of a wall, m

Greek Letters

ε = void space of the bed
ε_{mf}, ε_w = void fraction at the minimum fluidizing bed and at the wall layer
φ_w = ratio of effective thickness of gas film around a contact point to particle diameter for contact between particle and surface
φ_b = ratio of effective thickness of gas film around a contact point to particle diameter for contact between adjacent particles
η_j = effectiveness factor of jth reaction
η_{MS} = effectiveness factor of the methanol synthesis reaction
η_{WGS} = effectiveness factor of the water gas shift reaction
η_{MD} = effectiveness factor of the methanol dehydration reaction
μ, μ_a = dynamic viscosity and absolute viscosity, kg m^{-1} h^{-1}
ρ, ρ_g = fluid density, kg m^{-3}
ρ_b = bulk density of the bed, kg m^{-3}
ρ_p, ρ_{p1}, ρ_{p2} = particle density of hybrid catalyst, MeOH synthesis catalyst, and MeOH dehydration catalyst, respectively, g m^{-3}
ρ_w = cooling water density, kg m^{-3}
υ = fluid line velocity, m s^{-1}
υ_w = cooling water line velocity, m s^{-1}
$\sum v_i$ = diffusion volume, mol cm^{-3}
τ_t = residence time, h
$\gamma_{i,j}$ = stoichiometric coefficient of the ith component in the jth reaction

Literature Cited

(1) Semelsberger, T. A.; Borup, R. L.; Greene, H. L. Dimethyl ether (DME) as an alternative fuel. *J. Power Sources* **2006**, *156*, 497.

(2) Alam, M.; Fujita, O.; Ito, K. Performance of NO_x reduction catalysts with simulated dimethyl ether diesel engine exhaust gas. *Proc. Inst. Mech. Eng., Part A: J. Power Energy* **2004**, *218*, 89.

(3) Sorenson, S. C. Dimethyl ether in diesel engines: Progress and perspectives. *J. Eng. Gas Turbines, Power Trans. ASME* **2001**, *123*, 652.

(4) Rouhi, A. M. AMOCO, HALDOR-TOPSOE. Develop Dimethyl Ether As Alternative Diesel Fuel. *Chem. Eng. News.* **1995**, *73*, 37.

(5) Fleisch, T. H.; Basu, A.; Gradassi, M. J.; Masin, J. G. Dimethyl ether: A fuel for the 21st century. *Natural Gas Convers. IV: Stud. Surf. Sci. Catal.* **1995**, *107*, 17.

(6) Kaiser, E. W.; Wailington, T. J.; Hurley, M. D.; Platz, J.; Curran, H. J.; Pitz, W. J.; Westerbrook, C. K. Experimental and modelling study of premixed atmospheric-pressure dimethyl ether−air flames. *J. Phys. Chem. A* **2000**, *104*, 8194.

(7) Song, J.; Huang, Z.; Qiao, X. Q.; Wang, W. L. Performance of a controllable premixed combustion engine fueled with dimethyl ether. *Energy Convers. Manage.* **2004**, *45*, 2223.

(8) Wang, H. W.; Zhou, L. B. Performance of a direct injection diesel engine fuelled with a dimethyl ether/diesel blend. *Proc. Inst. Mech. Eng., Part D: J. Automobile Eng.* **2003**, *217*, 819.

(9) Zannis, T. C.; Hountalas, D. T. DI diesel engine performance and emissions from the oxygen enrichment of fuels with various aromatic content. *Energy Fuels* **2004**, *18*, 659.

(10) Peng, X. D.; Wang, A. W.; Toseland, B. A.; Tijm, P. J. A. Single-Step Syngas-to-Dimethyl Ether Processes for Optimal Productivity Minimal Emissions, and Natural Gas-Derived Syngas. *Ind. Eng. Chem. Res.* **1999**, *38*, 4381.

(11) Sun, K. P.; Lu, W. W.; Qiu, F. Y.; Liu, S. W.; Xu, X. L. Direct synthesis of DME over bifunctional catalyst: Surface properties and catalytic performance. *Appl. Catal., A* **2003**, *252*, 243.

(12) Omata, K.; Watanabe, Y.; Umegaki, T.; Ishiguro, G.; Yamada, M. Low-pressure DME synthesis with Cu-based hybrid catalysts using temperature-gradient reactor. *Fuel* **2002**, *81*, 1605.

(13) Shahrokhi, M.; Baghmisheh, G. R. Modeling, simulation and control of a methanol synthesis fixed-bed reactor. *Chem. Eng. Sci.* **2005**, *60*, 4275.

(14) Ng, K. L.; Chadwick, D.; Toseland, B. A. Kinetics and modelling of dimethyl ether synthesis from synthesis gas. *Chem. Eng. Sci.* **1999**, *54*, 3587.

(15) Vanden Busshe, K. M.; Froment, G. F. A steady-state kinetic model for methanol synthesis and the water gas shift reaction on a commercial $Cu/ZnO/Al_2O_3$ catalyst. *J. Catal.* **1996**, *161*, 1.

(16) Bercic, G.; Levec, J. Intrinsic and Global reaction rate of methanol dehydration over γ-Al_2O_3 pellets. *Ind. Eng. Chem. Res.* **1992**, *31*, 1035.

(17) Martyn, V.; Twigg. *Catalyst Handbook*; Wolfe: London, 1986.

(18) Stull, D. R.; Westrum, E. F.; Sinke, G. C. *The Chemical Thermodynamics of Organic Compounds*; John Wiley: New York, 1969.

(19) Kunii, D.; Levenspiel, O. *Fluidization Engineering*; Butterworth-Heinemann: Boston, MA, 1990.

(20) Welty, J. R.; Wicks, C. E.; Wilson, R. E. *Fundamentals of momentum, heat and mass transfer*; Wiley: New York, 1976.

(21) Cengel. *Heat transfer a practical approach*; McGraw Hill: Boston, MA, 1998.

(22) Satterfield, C. N. *Mass Transfer in Heterogeneous Catalysis*; M.I.T. Press: Cambridge, MA, 1970.

(23) Riggs, J. M. *An introduction to numerical methods for chemical engineers*; Texas Tech University Press: Lubbock, TX, 1994.

(24) McCabe, W. L.; Smith, J. C.; Harriott, P. *Unit Operations of Chemical Engineering*; McGraw Hill: New York, 1995.

(25) Poling, B. E.; Prausnitz, J. M.; O'Connell, J. P. *The Properties of Gases & Liquids*; McGraw Hill: New York, 2001.

(26) Perry, R. H.; Green, D. W. *Perry's Chemical Engineering Handbook*; McGraw Hill: New York, 1997.

(27) Fuller, E. N.; Schettler, P. D.; Giddings, J. C. A new method for prediction of binary gas-phase diffusion coefficients. *Ind. Eng. Chem.* **1966**, *58*, 19.

Received for review November 22, 2007
Revised manuscript received March 17, 2008
Accepted April 1, 2008

IE071589E